Spin-Orbit Coupling in Hydrogenated Graphene

Martin Gmitra, Denis Kochan, and Jaroslav Fabian
Institute for Theoretical Physics, University of Regensburg, 93040 Regensburg, Germany
(Received 10 March 2013; published 13 June 2013)

First-principles calculations of the spin-orbit coupling in graphene with hydrogen adatoms in dense and dilute limits are presented. The chemisorbed hydrogen induces a giant local enhancement of spin-orbit coupling due to sp^3 hybridization which depends strongly on the local lattice distortion. Guided by the reduced symmetry and the local structure of the induced dipole moments, we use group theory to propose realistic minimal Hamiltonians that reproduce the relevant spin-orbit effects for both single-side semihydrogenated graphene (graphone) and for a single hydrogen adatom in a large supercell. The principal linear spin-orbit band splittings are driven by the breaking of the local pseudospin inversion symmetry and the emergence of spin flips on the same sublattice.

DOI: 10.1103/PhysRevLett.110.246602 PACS numbers: 72.80.Vp, 71.70.Ej, 73.22.Pr

Spin-orbit coupling is central for a variety of spintronics phenomena [1,2] such as spin relaxation, spin transport, or topological quantum spin Hall effects. Itinerant electrons in graphene have weak spin-orbit coupling, as they are formed primarily from p_z orbitals which have zero orbital momentum. The Dirac cones are separated by what is called the intrinsic spin-orbit coupling of $2\lambda_{\mathrm{I}} = 24\ \mu$eV due to p_z-d mixing [3–6]. This small value is desirable for long spin lifetimes, but experiments suggest [7–10] that spin relaxation is governed by either much stronger spin-orbit or magnetic [11,12] interactions. Potential culprits are light adatoms [13–16], which are typically not important for momentum scattering but may be essential for spin-flip scattering. On the other hand, large spin-orbit coupling is important for the spin Hall effect [17] and for engineering robust quantum topological phases in graphene by heavy adatoms [18–20].

Hydrogen is an ideal light adatom to study induced spin effects in graphene. Not only can it produce local magnetic moments [21–24], as recently experimentally demonstrated [25], but it should also enhance graphene's spin-orbit coupling (SOC), as proposed in Ref. [13]. We show that while the general reason for the enhancement is sp^3 hybridization, specifically, the principal enhancement appears due to pseudospin inversion asymmetry (PIA), which generates novel spin-orbit couplings for conduction electrons.

The presence of both magnetic moment and large spin-orbit coupling makes the spin physics exciting but also challenging to explain spin-relaxation experiments (such as the recently observed increase in the spin-relaxation time due to hydrogenation [26]). To disentangle the two contributions, as well as to see what new phenomena they can lead to, it is important to consider them separately. Here, we present a quantitative and qualitative study of SOC induced by hydrogen on graphene in two limits. One is the dense limit, represented here by single-side semihydrogenated graphene (also called graphone) [27]. This structure is relatively simple and allows for a quantitative analysis of the sp^3 hybridization effects on various spin-orbit parameters. Our results indeed show a giant enhancement of SOC, strongly dependent on the buckling deformations of this structure. We introduce single-band and tight-binding Hamiltonians to describe the main SOC effects.

We also quantify the local spin-orbit structure and propose a minimal realistic SOC Hamiltonian in the dilute limit, represented by large supercells (starting with 5×5), intensively studied for orbital effects [28–31]. Based on first-principles calculations, we demonstrate a giant local—and we identify the local impurity region from the dipole moments distribution—enhancement of SOC due to sp^3 hybridization and formulate a minimal realistic SOC hopping model for the first time. We believe that this is a benchmark model to study spin relaxation, spin transport, but also mesoscopic quantum interference [11,32] phenomena in which spin-flip and spin-orbit scattering play an important role. Our results are in general agreement with the finding of the recent experiment on the spin Hall effect in hydrogenated graphene [17] in which large spin-orbit coupling was deduced. The present theory gives foundations to study such phenomena in a quantitative way.

Dense limit: Single-side semihydrogenated graphene (SHG).—The effects of sp^3 hybridization on SOC are studied using single-side semihydrogenated graphene [inset in Fig. 1(a)] with different degrees of out-of-plane lattice distortion Δ of the hydrogenated carbon site which is on sublattice A. The C-H bond length d_{H} is 1.13 Å, and we take the lattice constant to be $a \approx 2.516$ Å, which is the relaxed distance between the nearest neighbors at the adatom site in a 5×5 supercell discussed below; in graphene, the lattice constant is 2.46 Å. (The relaxed SHG structure of lattice constant 2.535 Å would have $\Delta/a = 9.7\%$ and the sp^3 tetrahedron 20.41%.) In examples, we choose $\Delta/a = 14\%$, which corresponds to relaxed large supercell structures.

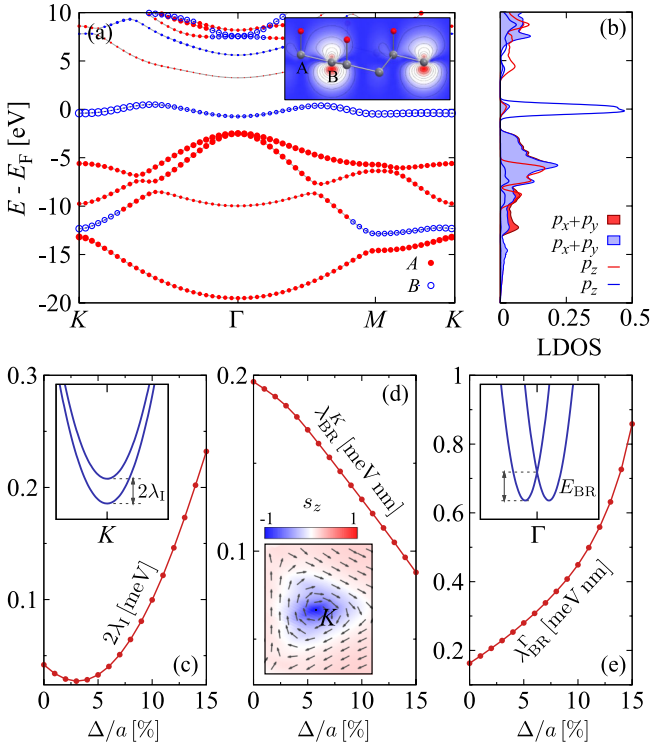

FIG. 1 (color online). Top: Calculated electronic band structure of single-side semihydrogenated graphene. (a) Sublattice resolved band structure for the distortion $\Delta/a = 14\%$. The filled (red) circles correspond to sublattice A, whereas the open (blue) circles correspond to sublattice B. The circles' radii correspond to the carbon atom charge densities. The inset shows the structure and the probability density of the flat band at the K point. (b) Orbital resolved local density of states (LDOS). Bottom: Extracted spin-orbit coupling parameters for the π^* band at K and Γ as functions of Δ/a. (c) Intrinsic spin-orbit coupling splitting $2\lambda_I$ at K. The inset shows the band splitting. (d) Adatom-induced SOC splitting λ^K_{BR} at K. The inset shows the spin texture around K for the lower spin-orbit split band. The in-plane components are shown by the arrows, while the z component is shown by the color map. (e) Adatom-induced SOC splitting λ^Γ_{BR} at Γ. The inset shows the band splitting around Γ with the identified Bychkov-Rashba energy $E_{BR} = 0.87\ \mu$eV for $\Delta/a = 14\%$.

To study SOC effects, we restrict the computational basis to be spin unpolarized. The calculated electronic structure and the projected local density of states for SHG are shown in Fig. 1 (top) for $\Delta/a = 14\%$. Compared to graphene, in which π and π^* bands without SOC touch at K [33], the C-H bonding pulls them apart: the π band, which at K comes mainly from sublattice A, is shifted to about 5 eV below the Fermi level (the GW approximation predicts a greater shift by about 2 eV [22]). The π^* band, which comes from sublattice B, lies at the Fermi level. This band, which we consider for our SOC analysis, is narrow since the nearest-neighbor hopping is inhibited for p_z electrons on B. The inset in Fig. 1(a) shows the π^* probability density at K that has the p_z character on sublattice B.

We now extract the SOC parameters for the states at K and Γ for the π^* band which is at the Fermi level. Since this band is nondegenerate, the effective spin-orbit Hamiltonian can be expressed via the spin Pauli matrices $\hat{s}$. The small group of K (Γ) is C_3 (C_{3v}). Up to terms linear in momentum, which is here measured from K and Γ, the SOC Hamiltonians compatible with those symmetries are

$$\mathcal{H}^{\tau K}_{\rm eff} = \lambda^K_{\rm BR}(k_x\hat{s}_y - k_y\hat{s}_x) + \tau\lambda_{\rm I}\hat{s}_z, \tag{1}$$

$$\mathcal{H}^{\Gamma}_{\rm eff} = \lambda^\Gamma_{\rm BR}(k_y\hat{s}_x - k_x\hat{s}_y). \tag{2}$$

Here, $\tau = 1$ (-1) stands for K (K'), $\lambda_{\rm I}$ is the adatom-modified intrinsic spin-orbit coupling, and $\lambda_{\rm BR}$ is the adatom-induced (Bychkov-Rashba-like, as in semiconductor physics [34]) spin-orbit coupling. We will see that the latter comes from the space and pseudospin inversion asymmetry. Contrary to graphene, the BR SOC at K depends on the momentum magnitude. Higher-order terms in $\mathcal{H}^{\tau K}_{\rm eff}$ and $\mathcal{H}^{\Gamma}_{\rm eff}$ are presented in [35].

Figure 1 (bottom) shows the extracted SOC parameters as functions of Δ/a. The intrinsic SOC $\lambda_{\rm I}$ is obtained from the splitting of the band at K; see the inset in Fig. 1(c). The parameter $\lambda^K_{\rm BR}$ is extracted by fitting the linear dependence of the ratio of the spin-expectation values $\langle\hat{s}_x\rangle/\langle\hat{s}_z\rangle|_{k_x=0} = \lambda^K_{\rm BR}k_y/\lambda_{\rm I} + O(k_y^3)$ close to K. The trigonally warped spin texture around K is shown in the inset of Fig. 1(d) and can be described by higher-order terms in $\mathcal{H}^{\tau K}_{\rm eff}$ [35]. Finally, $\lambda^\Gamma_{\rm BR}$ is obtained by fitting the spin splitting at Γ; see the inset in Fig. 1(e). SOC is significantly enhanced in comparison to graphene. Directly comparable is the intrinsic SOC parameter whose value in graphene is $2\lambda_{\rm I} = 24\ \mu$eV [3].

The above single-band model can be obtained from a tight-binding (TB) Hamiltonian using the carbon p_z and hydrogen s orbital basis. The Hamiltonian contains orbital and SOC parts $\mathcal{H} = \mathcal{H}_{\rm orb} + \mathcal{H}_{\rm so}$. We denote by $c^\dagger_{i\sigma} = (a^\dagger_{i\sigma}, b^\dagger_{i\sigma})$ and $c_{i\sigma} = (a_{i\sigma}, b_{i\sigma})$ the creation and annihilation operators for the p_z orbitals on the sublattices (A, B), with spin σ and lattice site i. Similarly, we define $h^\dagger_{m\sigma}$ and $h_{m\sigma}$ for the hydrogen s orbitals on adatom sites m. For the orbital part $\mathcal{H}_{\rm orb}$, we take the TB model Hamiltonian introduced in Refs. [30,36], which assumes the nearest-neighbor carbon-carbon (C-C) hopping $t = 2.6$ eV, direct carbon-hydrogen (C-H) hopping T, and the adatom on-site energy ε_h:

$$\mathcal{H}_{\rm orb} = \varepsilon_h\sum_m h^\dagger_{m\sigma}h_{m\sigma} - t\sum_{\langle i,j\rangle} c^\dagger_{i\sigma}c_{j\sigma} + T\sum_{\langle m,i\rangle} h^\dagger_{m\sigma}c_{i\sigma} + \text{H.c.} \tag{3}$$

The angle brackets denote the nearest neighbors. Fitting the TB model to the first-principles band structure for $\Delta/a = 14\%$ (distortion in the single-adatom limit, see below), we obtain $\varepsilon_h = 3$ eV and $T = 6.5$ eV. The values

are reliable in the vicinity of the K point, where p_z carbon orbitals dominate the projected local density of states.

The SOC Hamiltonian can be derived by inspecting the reduction of the graphene point group symmetry D_{6h}—which allows for the intrinsic spin-orbit coupling λ_{I} only—to the one corresponding to SHG. First, the C-H covalent bonds break the space inversion symmetry and the point group reduces to C_{6v}. This structure inversion asymmetry induces the Bychkov-Rashba-like term Λ_{BR}. Second, the hydrogenated carbons on sublattice A cannot be interchanged with the nonhydrogenated carbons on sublattice B. This breaks the pseudospin inversion symmetry, and $C_{6v} \to C_{3v}$. The effect of the latter reduction is twofold: (i) The intrinsic SOC depends on the sublattice Λ_{I}^{A} and Λ_{I}^{B}, and (ii) new SOC terms emerge due to the pseudospin inversion asymmetry $\Lambda_{\mathrm{PIA}}^{A}$ and $\Lambda_{\mathrm{PIA}}^{B}$ discussed below.

As the hydrogen s orbitals do not directly contribute to SOC, we can express the SOC TB Hamiltonian in the p_z basis. In the next-nearest-neighbor limit, this Hamiltonian has five real parameters and reads

$$\mathcal{H}_{\mathrm{so}} = \frac{2i}{3}\sum_{\langle i,j\rangle} c_{i\sigma}^{\dagger} c_{j\sigma'} [\Lambda_{\mathrm{BR}}(\hat{\boldsymbol{s}} \times \mathbf{d}_{ij})_z]_{\sigma\sigma'} + \frac{i}{3}\sum_{\langle\langle i,j\rangle\rangle} c_{i\sigma}^{\dagger} c_{j\sigma'} \left[\frac{\Lambda_{\mathrm{I}}^{c}}{\sqrt{3}}\nu_{ij}\hat{s}_z + 2\Lambda_{\mathrm{PIA}}^{c}(\hat{\boldsymbol{s}} \times \mathbf{D}_{ij})_z\right]_{\sigma\sigma'}. \tag{4}$$

The double angular brackets stand for the next-nearest neighbors, and the label c denotes sublattice A or B. Factors $\nu_{ij} = 1$ (-1) stay for the clockwise (counterclockwise) hopping path j to i. The nearest-neighbor $\mathbf{d}_{ij}$ and next-nearest-neighbor $\mathbf{D}_{ij}$ unit vectors point from j to i (in a flat lattice). The first term in Eq. (4) is the standard Bychkov-Rashba hopping as for graphene. The second term describes the sublattice resolved intrinsic SOC which couples the same spins and the PIA term which couples opposite spins on the same sublattice. The Hamiltonian $\mathcal{H}_{\mathrm{so}}$ in Eq. (4) applies to any hexagonal lattice system with C_{3v} point group symmetry, such as boron nitride or silicene in a transverse electric field.

The single-band limit described by Eq. (1) can be obtained from the TB Hamiltonian $\mathcal{H} = \mathcal{H}_{\mathrm{orb}} + \mathcal{H}_{\mathrm{so}}$ by downfolding to sublattice B; for a general perturbative downfolding scheme, see [37]. In our case, it can be done in two steps; getting rid of the hydrogen s orbitals $\mathcal{H}_{\mathrm{orb}} + \mathcal{H}_{\mathrm{so}} \to \sum_i (T^2/\varepsilon_h) a_{i\sigma}^{\dagger} a_{i\sigma} - t\sum_{\langle i,j\rangle} c_{i\sigma}^{\dagger} c_{j\sigma} + \mathcal{H}_{\mathrm{so}}$; in effect, the sublattice A acquires a staggered on-site potential. When transforming this downfolded Hamiltonian to the carbon atom Bloch basis, we get an effective 4×4 Bloch Hamiltonian. Repeating now the downfolding procedure with sublattice A states, we arrive at the 2×2 Hamiltonian $\mathcal{H}_{\mathrm{eff}}(\mathbf{k})$. Expanding $\mathcal{H}_{\mathrm{eff}}(\mathbf{k})$ near the K (K') point gives in the leading order $\mathcal{H}_{\mathrm{eff}}^{\tau K}$ [see Eq. (1)], with

$$\lambda_{\mathrm{BR}}^{K} \simeq -a\Lambda_{\mathrm{PIA}}^{B} - \sqrt{3}a\Lambda_{\mathrm{BR}}\frac{t\varepsilon_h}{T^2}, \tag{5}$$

$$\lambda_{\mathrm{I}} \simeq -\Lambda_{\mathrm{I}}^{B} - 2\frac{\Lambda_{\mathrm{BR}}^{2}\varepsilon_h}{T^2}. \tag{6}$$

Both PIA and BR SOC hopping terms contribute to the effective band SOC parameters. This is the likely reason for the extracted nonmonotonic dependence of λ_{I} and the decrease of $\lambda_{\mathrm{BR}}^{K}$ as a function of Δ/a, shown in Fig. 1 (bottom). The TB model cannot be reliably used at Γ as there other bands (orbitals) mix in; see Fig. 1(a) and Ref. [35].

We also present an effective SOC Hamiltonian close to K. After transforming $\mathcal{H}_{\mathrm{so}}$ to the ordered Bloch basis $[\psi_{A\uparrow}(k), \psi_{A\downarrow}(k), \psi_{B\uparrow}(k), \psi_{B\downarrow}(k)]$ and linearizing near K (K'), we obtain

$$\mathcal{H}_{\mathrm{so}}^{\tau K} = \Lambda_{\mathrm{BR}}(\tau\hat{\sigma}_x\hat{s}_y - \hat{\sigma}_y\hat{s}_x) + \tfrac{1}{2}[\Lambda_{\mathrm{I}}^{A+B}\hat{\sigma}_z + \Lambda_{\mathrm{I}}^{A-B}\hat{\sigma}_0]\tau\hat{s}_z + \tfrac{1}{2}[\Lambda_{\mathrm{PIA}}^{A+B}\hat{\sigma}_z + \Lambda_{\mathrm{PIA}}^{A-B}\hat{\sigma}_0]a(k_x\hat{s}_y - k_y\hat{s}_x). \tag{7}$$

Here, $(\hat{\sigma}_0, \hat{\boldsymbol{\sigma}})$ and $(\hat{s}_0, \hat{\boldsymbol{s}})$ stand for the unit and Pauli matrices in the pseudospin and spin spaces, respectively. The momentum is measured form K (K') and parameters $\Lambda^{A\pm B} = \Lambda^{A} \pm \Lambda^{B}$. If z-inversion symmetry is restored, Λ_{BR}, $\Lambda_{\mathrm{PIA}}^{A+B}$, and $\Lambda_{\mathrm{I}}^{A-B}$ vanish and one obtains the silicene limit [38].

Hydrogen on a supercell: Single-adatom limit.—The single-adatom limit is represented by a 5×5 supercell with a single hydrogen (2% coverage). We use a fully relaxed structure with $\Delta \approx 0.36$ Å (14% distortion) and the next-nearest-neighbor distance $a = 2.516$ Å of the carbon atoms around the hydrogenated site $\mathrm{C_H}$.

Figure 2(a) shows the calculated spin-unpolarized electronic band structure of our 5×5 supercell. The low energy spectrum contains three characteristic bands: the valence and conduction bands and the midgap impuritylike band. These three bands can be nicely fitted by two parameters $T = 7.5$ eV and $\varepsilon_h = 0.16$ eV entering the Hamiltonian $\mathcal{H}_{\mathrm{orb}}$ [Eq. (3)], as seen in Fig. 2(a). Our values differ from Refs. [30,36]; the comparison is discussed in [35]. Larger supercells are also well described by these parameters, confirming that the 5×5 one already describes the dilute limit; see [35]. The TB model with s and p_z orbitals is also supported by the projected p_z local density of states per carbon atoms around the hydrogenated carbon as compared to the total density of states; see Fig. 2(b).

The calculated spin-orbit splittings are shown in Fig. 2(c). To explain them, we propose a minimal realistic SOC model which is locally C_{3v} invariant in the impurity region with the C-H bond as the threefold axis of symmetry. We deduce the impurity region from the induced dipole moments, shown in Fig. 3(a). The main effects are confined up to the second-nearest neighbors of the hydrogenated site $\mathrm{C_H}$ (in sublattice A), defining our impurity region. We use $A_{\sigma}^{\dagger}$ (A_{σ}) for the creation (annihilation) operators

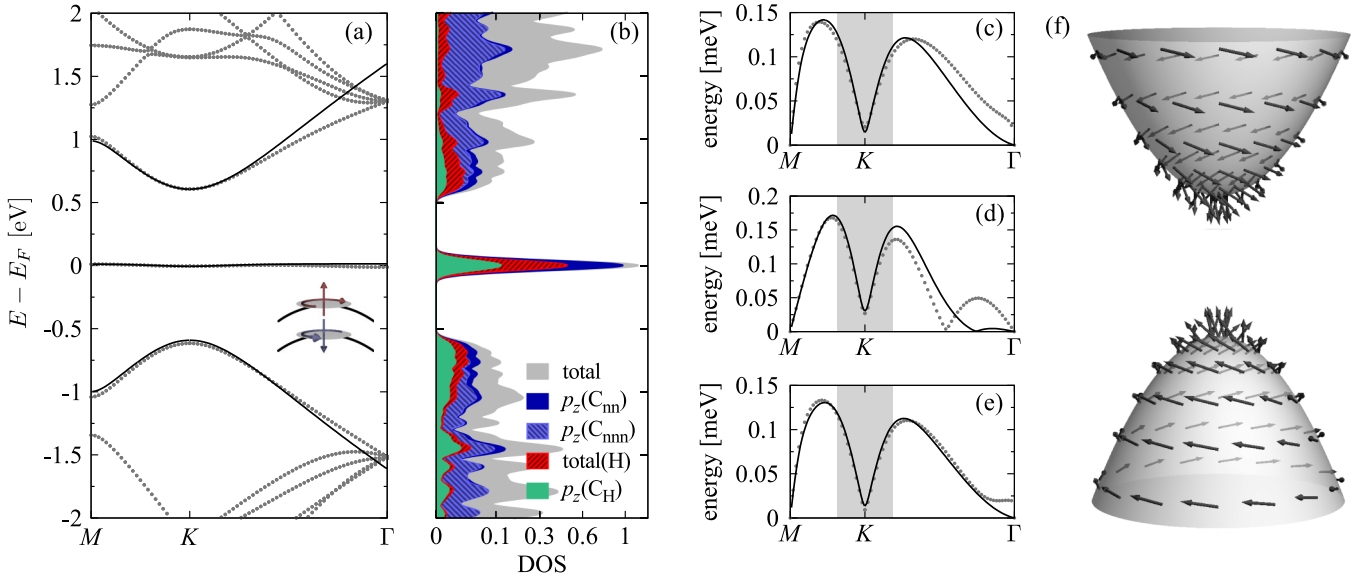

FIG. 2 (color online). First-principles results and their tight-binding model fits for a hydrogen adatom on a 5×5 supercell. (a) Electronic band structure around the Fermi level. The dots are first-principles results, and the solid lines are tight-binding model fits. The band spin-orbit splitting around K is sketched for the valence band, indicating the out-of-plane z components and the rotation directions of the in-plane spin components. (b) Broadened total density of states per atom (gray areas) and p_z projected local densities for atoms in the vicinity of the adatom: C_H the hydrogenated carbon atom (shown in green), C_{nn} its nearest neighbor (in dark blue), C_{nnn} the next-nearest neighbor (in light blue), and the total density on hydrogen H (in red). The projected densities of states are normalized to the corresponding number of atoms in the set. (c) Conduction, (d) impurity, and (e) valence band spin-orbit splittings along the high-symmetry lines; the symbols are as in (a). Tight-binding model least-squares fits are performed within the shaded regions around K. (f) Spin-expectation values around K for the spin-orbit split valence and conduction bands closer to the Fermi level.

on C_H and $B^\dagger_{m,\sigma}$ ($B_{m,\sigma}$) on the three nearest neighbors. Otherwise, the terminology follows the SHG case. The SOC Hamiltonian compatible with the local symmetry is

$$\begin{aligned}\mathcal{H}_{so} = {} & \frac{i}{3}\sum_{\langle\langle i,j\rangle\rangle}{}' c^\dagger_{i\sigma} c_{j\sigma'}\left[\frac{\lambda_I}{\sqrt{3}}\nu_{ij}\hat{s}_z\right]_{\sigma\sigma'} \\ & + \frac{i}{3}\sum_{\langle\langle C_H,j\rangle\rangle} A^\dagger_\sigma c_{j\sigma'}\left[\frac{\Lambda_I}{\sqrt{3}}\nu_{C_H,j}\hat{s}_z\right]_{\sigma\sigma'} + \text{H.c.} \\ & + \frac{2i}{3}\sum_{\langle C_H,j\rangle} A^\dagger_\sigma B_{j\sigma'}[\Lambda_{BR}(\hat{s}\times\mathbf{d}_{C_H,j})_z]_{\sigma\sigma'} + \text{H.c.} \\ & + \frac{2i}{3}\sum_{\langle\langle i,j\rangle\rangle} B^\dagger_{i\sigma} B_{j\sigma'}[\Lambda_{PIA}(\hat{s}\times\mathbf{D}_{ij})_z]_{\sigma\sigma'}. \end{aligned} \quad (8)$$

The first term is the graphene intrinsic SOC ($2\lambda_I = 24\ \mu$eV). It couples all next-nearest-neighbor pairs not containing C_H. (This is denoted by the primed summation symbol.) The second term describes the adatom-induced intrinsic spin-orbit coupling Λ_I, which couples the same spins on the same sublattice. The third term, with the Bychkov-Rashba hopping parameter Λ_{BR}, describes the induced nearest-neighbor spin flips. Finally, the fourth term, with the PIA parameter Λ_{PIA}, comes from the pseudospin inversion asymmetry. This term couples opposite spins of the next-nearest neighbors. We remark that C_{3v} symmetry allows more spin-orbit hopping terms in our impurity region. We considered them all but found only the three Λ's in Eq. (8) relevant to explain our *ab initio* results; see the scheme in Fig. 3(b).

Figures 2(c)–2(e) show spin-orbit coupling induced band splittings along high-symmetry lines. The multiband least-squares fit around the K point gives the following values for the SOC parameters: $\Lambda_I = -0.21$ meV, which is about 17 times larger than that of graphene λ_I; $\Lambda_{BR} = 0.33$ meV, more than 60 times the value in graphene where $\lambda_{BR} = 5\ \mu$eV in a representative transverse electric field of 1 V/nm [3]; and $\Lambda_{PIA} = -0.77$ meV, which has no counterpart in flat graphene. The signs of the above parameters

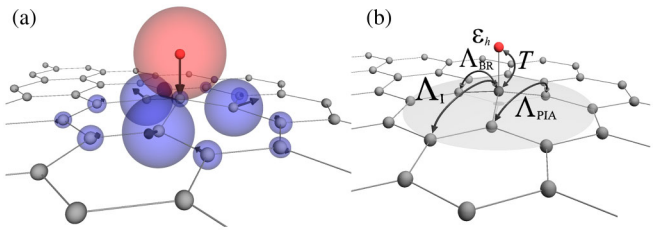

FIG. 3 (color online). (a) First-principles calculations of electric dipole moments induced by hydrogen adatoms on a 5×5 supercell. The directions of the dipole moments are shown by arrows; the sphere radii correspond to the dipole magnitudes. (b) Hopping scheme of the tight-binding model showing the relevant orbital and spin-orbit coupling parameters.

have been determined from the spin-expectation values around the K point, shown in Fig. 2(f). The spin texture is governed mainly by PIA SOC. Those parameters also fit larger supercells [35], and we propose them, together with Hamiltonian Eq. (8), to describe the single adatom limit important for investigating spin-flip and spin-orbit scattering in graphene. Our parameters roughly agree with the extracted value of (some effective) spin-orbit coupling in hydrogenated graphene of 1.25 eV [17], but the presence of PIA suggests that the modeling of spin Hall and spin-relaxation effects in hydrogenated graphene needs refining.

In conclusion, we investigated spin-orbit coupling induced by hydrogen, representing light adatoms, on graphene in dense and dilute limits. We introduced realistic spin-orbit coupling model Hamiltonians and provided quantitative values for their parameters that can be used to study spin relaxation, spin transport, and mesoscopic transport in graphene with adatoms or in similar two-dimensional structures of the same symmetry.

We thank T. O. Wehling for helpful discussions. This work was supported by the DFG SFB 689, SPP 1285, and GRK 1570.

[1] I. Žutić, J. Fabian, and S. Das Sarma, Rev. Mod. Phys. **76**, 323 (2004).
[2] J. Fabian, A. Matos-Abiague, C. Ertler, P. Stano, and I. Žutić, Acta Phys. Slovaca **57**, 565 (2007).
[3] M. Gmitra, S. Konschuh, C. Ertler, C. Ambrosch-Draxl, and J. Fabian, Phys. Rev. B **80**, 235431 (2009).
[4] S. Konschuh, M. Gmitra, and J. Fabian, Phys. Rev. B **82**, 245412 (2010).
[5] S. Konschuh, M. Gmitra, D. Kochan, and J. Fabian, Phys. Rev. B **85**, 115423 (2012).
[6] S. Abdelouahed, A. Ernst, J. Henk, I. V. Maznichenko, and I. Mertig, Phys. Rev. B **82**, 125424 (2010).
[7] N. Tombros, C. Józsa, M. Popinciuc, H. T. Jonkman, and B. J. van Wees, Nature (London) **448**, 571 (2007).
[8] K. Pi, W. Han, K. M. McCreary, A. G. Swartz, Y. Li, and R. K. Kawakami, Phys. Rev. Lett. **104**, 187201 (2010).
[9] T.-Y. Yang, J. Balakrishnan, F. Volmer, A. Avsar, M. Jaiswal, J. Samm, S. R. Ali, A. Pachoud, M. Zeng, M. Popinciuc, G. Güntherodt, B. Beschoten, and B. Özyilmaz, Phys. Rev. Lett. **107**, 047206 (2011).
[10] R. G. Mani, J. Hankinson, C. Berger, and W. A. de Heer, Nat. Commun. **3**, 996 (2012).
[11] M. B. Lundeberg, R. Yang, J. Renard, and J. A. Folk, Phys. Rev. Lett. **110**, 156601 (2013).
[12] A. A. Kozikov, D. W. Horsell, E. McCann, and V. I. Fal'ko, Phys. Rev. B **86**, 045436 (2012).
[13] A. H. Castro Neto and F. Guinea, Phys. Rev. Lett. **103**, 026804 (2009).
[14] C. Ertler, S. Konschuh, M. Gmitra, and J. Fabian, Phys. Rev. B **80**, 041405 (2009).
[15] P. Zhang and M. W. Wu, New J. Phys. **14**, 033015 (2012).
[16] D. V. Fedorov, M. Gradhand, S. Ostanin, I. V. Maznichenko, A. Ernst, J. Fabian, and I. Mertig, Phys. Rev. Lett. **110**, 156602 (2013).
[17] J. Balakrishnan, G. K. W. Koon, M. Jaiswal, A. H. Castro Neto, and B. Özyilmaz, Nat. Phys. **9**, 284 (2013).
[18] Z. Qiao, S. A. Yang, W. Feng, W.-K. Tse, J. Ding, Y. Yao, J. Wang, and Q. Niu, Phys. Rev. B **82**, 161414 (2010).
[19] C. Weeks, J. Hu, J. Alicea, M. Franz, and R. Wu, Phys. Rev. X **1**, 021001 (2011).
[20] H. Zhang, C. Lazo, S. Blügel, S. Heinze, and Y. Mokrousov, Phys. Rev. Lett. **108**, 056802 (2012).
[21] O. V. Yazyev, Phys. Rev. Lett. **101**, 037203 (2008).
[22] G. Fiori, S. Lebègue, A. Betti, P. Michetti, M. Klintenberg, O. Eriksson, and G. Iannaccone, Phys. Rev. B **82**, 153404 (2010).
[23] J. O. Sofo, G. Usaj, P. S. Cornaglia, A. M. Suarez, A. D. Hernández-Nieves, and C. A. Balseiro, Phys. Rev. B **85**, 115405 (2012).
[24] D. Soriano, N. Leconte, P. Ordejón, J. C. Charlier, J. J. Palacios, and S. Roche, Phys. Rev. Lett. **107**, 016602 (2011).
[25] K. M. McCreary, A. G. Swartz, W. Han, J. Fabian, and R. K. Kawakami, Phys. Rev. Lett. **109**, 186604 (2012).
[26] M. Wojtaszek, I. J. Vera-Marun, T. Maassen, and B. J. van Wees, Phys. Rev. B **87**, 081402 (2013).
[27] J. Zhou, Q. Wang, Q. Sun, X. S. Chen, Y. Kawazoe, and P. Jena, Nano Lett. **9**, 3867 (2009).
[28] E. J. Duplock, M. Scheffler, and P. J. D. Lindan, Phys. Rev. Lett. **92**, 225502 (2004).
[29] V. M. Pereira, F. Guinea, J. M. B. Lopes dos Santos, N. M. R. Peres, and A. H. Castro Neto, Phys. Rev. Lett. **96**, 036801 (2006).
[30] J. P. Robinson, H. Schomerus, L. Oroszlány, and V. I. Fal'ko, Phys. Rev. Lett. **101**, 196803 (2008).
[31] T. O. Wehling, S. Yuan, A. I. Lichtenstein, A. K. Geim, and M. I. Katsnelson, Phys. Rev. Lett. **105**, 056802 (2010).
[32] E. McCann and V. I. Fal'ko, Phys. Rev. Lett. **108**, 166606 (2012).
[33] P. R. Wallace, Phys. Rev. **71**, 622 (1947).
[34] Y. A. Bychkov and E. I. Rashba, JETP Lett. **39**, 78 (1984).
[35] See Supplemental Material at http://link.aps.org/supplemental/10.1103/PhysRevLett.110.246602 for details of first-principles calculations and single-band spin-orbit Hamiltonian derivation.
[36] T. O. Wehling, M. I. Katsnelson, and A. I. Lichtenstein, Phys. Rev. B **80**, 085428 (2009).
[37] G. L. Bir and G. E. Pikus, *Symmetry and Strain-Induced Effects in Semiconductors* (Wiley, New York, 1974), Chap. 3.
[38] C.-C. Liu, H. Jiang, and Y. Yao, Phys. Rev. B **84**, 195430 (2011).